energies

MDPI

Article

Modified Activated Graphene-Based Carbon Electrodes from Rice Husk for Supercapacitor Applications

Mukhtar Yeleuov [1,2], Christopher Seidl [3], Tolganay Temirgaliyeva [2,4,*], Azamat Taurbekov [2,4], Nicholay Prikhodko [2,5], Bakytzhan Lesbayev [2,4], Fail Sultanov [2,4,*], Chingis Daulbayev [1,2,4,*] and Serik Kumekov [1]

1 Department of Engineering Physics, Satbayev University, Almaty 050013, Kazakhstan; m.yeleuov@satbayev.university (M.Y.); skumekov@mail.ru (S.K.)
2 Laboratory of Carbon Nanomaterials Synthesis in Flame, Institute of Combustion Problems, Almaty 050000, Kazakhstan; a.taurbek@gmail.com (A.T.); nik99951@mail.ru (N.P.); lesbayev@mail.ru (B.L.)
3 Faculty of Engineering & Natural Sciences, Johannes Kepler University Linz, 4040 Linz, Austria; seidl.ch@edumail.at
4 Faculty of Chemistry and Chemical Technology, al-Farabi Kazakh National University, Almaty 050000, Kazakhstan
5 Department of Management and Entrepreneurship, Almaty University of Power Engineering and Telecommunications, Almaty 050013, Kazakhstan
* Correspondence: tts@icp.kz (T.T.); sultanov.fail@kaznu.kz (F.S.); chingis.daulbayev@kaznu.kz (C.D.)

Received: 4 September 2020; Accepted: 17 September 2020; Published: 21 September 2020

Abstract: The renewable biomass material obtained from rice husk, a low-cost agricultural waste, was used as a precursor to synthesize a highly porous graphene-based carbon as electrode material for supercapacitors. Activated graphene-based carbon (AGC) was obtained by a two-step chemical procedure and exhibited a very high specific surface area (SSA) of 3292 m^2 g^{-1}. The surface morphology of the synthesized materials was studied using scanning and transmission electron microscopy (SEM, TEM). Furthermore, the AGC was modified with nickel hydroxide $Ni(OH)_2$ through a simple chemical precipitation method. It was found that the most significant increase in capacitance could be reached with $Ni(OH)_2$ loadings of around 9 wt.%. The measured specific capacitance of the pure AGC supercapacitor electrodes was 236 F g^{-1}, whereas electrodes from the material modified with 9 wt.% $Ni(OH)_2$ showed a specific capacitance of up to 300 F g^{-1} at a current density of 50 mA g^{-1}. The increase in specific capacitance achieved due to chemical modification was, therefore 27%.

Keywords: supercapacitor electrode; activated rice husk; few-layer graphene; nickel hydroxide

1. Introduction

Due to various problems such as air quality and climate change, the world's energy system is shifting from a fossil fuel-driven economy to renewable energy sources. The main known renewable energy sources, such as wind and solar energy, are strongly dependent on weather conditions. Therefore, with a growing share of renewable energy sources in the electricity grid, an increased amount of storage devices will be needed. Electrical energy storage devices must fulfil a wide variety of very different requirements, for example, securing grid stability and power quality in microsecond intervals for long-time storage of significant energy amounts for seasonal energy compensation [1]. Supercapacitors are promising devices for short-term energy storage due to their long-cycle life and fast charge–discharge processes [2]. Their characteristic properties make them particularly suitable for

applications, such as hold-up/bridging power to the grid or equipment, and in uninterruptible power supply devices or regenerative braking [3]. The energy storage capability of supercapacitors arises from two different mechanisms. The first mechanism, the so-called electrochemical double-layer capacitance (EDLC), is an outcome of the Helmholtz's formation of double layers at the electrode–electrolyte interface. Another kind of capacitance is pseudo-capacitance; in this case, the charge is stored via fast reversible surface redox reactions [2,4,5]. High SSA nanomaterials like porous carbon, carbon nanotubes, and graphene are applied to reach high capacitance values for EDLC [6–10]. Various methods to produce porous carbon from different kinds of raw materials have been reported; recent research has focused on the utilization of renewable carbon precursors. For many Asian countries, rice husk has been found to be a promising candidate as a renewable carbon precursor due to its great availability. However, the high amount of silica in rice husk is still challenging for the production of high EDLC electrode materials [11,12]. Procedures for obtaining graphene from rice husk have also been reported in [13–15]. Commonly studied pseudo-capacitive materials especially include transition metal oxides, such as NiO, MnO_2, CoO_3, etc. [9,16,17]. Supercapacitors based on pseudo-capacitive materials are not cyclically stable compared to carbon-based EDLC electrode materials. If both charge storage mechanisms, Faradaic and EDLC, are applied in a supercapacitor, increasing the specific capacitance while still holding a high cyclic stability is possible. Such devices are called hybrid supercapacitors. A device with two similar electrodes is designated as a symmetrical capacitor, whereas supercapacitors with different electrodes are so-called asymmetric capacitors [9].

Among numerous electrode materials for pseudo-capacitance, nickel hydroxide has also been found to be a promising candidate [18,19]. Different synthesis methods are possible for the production of nickel hydroxide with a wide range of various structures. The electrochemical activity of nickel hydroxide comes from the unpaired d-electrons or vacant d-orbital, which allows binding with foreign species. The reachable capacitance of nickel hydroxide electrode material strongly relies on its structure and surface, and therefore, on synthesizing the electrode material. Chemical vapor deposition, chemical bath deposition, chemical precipitation, and electrodeposition are procedures applied in the preparation of nickel hydroxide composite electrodes; the deposition of nickel hydroxide has already been studied on nickel foam, activated carbon, graphene, and carbon nanotubes [20–22].

In this work, we prepared mesoporous carbon from rice husk using a two-stage method, including pyrolysis carbonization and thermochemical activation. The AGC was then modified with nickel hydroxide particles using a simple chemical precipitation method. The pure AGC showed a high SSA, reaching 3292 $m^2\ g^{-1}$ in Brunauer–Emmett–Teller (BET) analyses. The capacitance of the pure AGC-based electrode material was 212 F g^{-1} at a scan rate of 1 mV s^{-1}. The biggest enhancement of capacitance was found for 9 wt.% $Ni(OH)_2$ in AGC, reaching 258 F g^{-1} at a scan rate of 1 mV s^{-1}, which is an increase by 22% compared to pure AGC. The specific capacitance obtained from cyclic voltammetry (CV) data was lower than that calculated from the galvanostatic charge-discharge (GCD) data, which has already been observed by previous authors.

2. Materials and Methods

2.1. Preparation of Activated Rice Husk

Low-cost renewable rice husk was used as a precursor to synthesize a highly porous activated graphene-based carbon. The AGC was obtained by performing a two-step procedure. First, the rice husk was washed and dried for 3 h at 120 °C. It was then transferred to a rotating tubular furnace and heated to 450 °C at a rate of 7.5 °C min^{-1} under inert atmosphere (Ar gas flow rate of 5 cubic centimeters per minute); the carbonization temperature was held for 90 min. The oven was allowed to cool to ambient temperature. Afterwards, the carbonized rice husk was mixed in a weight ratio of 1:4 with dry potassium hydroxide (KOH). The mixture was transferred to a vertical tubular furnace and heated to 850 °C at a rate of 8 °C min^{-1} under inert atmosphere (Ar gas flow rate of 5 cubic centimeters per minute); the activation temperature was held for 120 min. After the oven cooled down, activated

rice husk (ARH) with an excess of KOH was yielded. The sample was washed with distilled water to remove excess KOH until the pH reached approx. 6–7 and it was then dried at 120 °C for 10 h. This method can be extended to other biomass to produce AGC.

2.2. Modification with $Ni(OH)_2$

AGC in the amount of 0.3 g was dispersed in 0.1 molar nickel (II) nitrate solution, under continuous stirring at room temperature while 0.1 molar sodium hydroxide was added dropwise to the mixture. The volume ratio between 0.1 molar nickel (II) nitrate solution and 0.1 molar sodium hydroxide was 1:2. For the calculations, it was assumed that 100% of Ni was precipitated as $Ni(OH)_2$. After completing the addition of NaOH, the mixture was mixed for 15 h, then transferred into a glass dish and dried at 110 °C for 8 h.

2.3. Characterizations

The morphology and structure of the AGC were observed using SEM (Jeol JSM-6490LA), TEM (JEM-2100), and Raman spectroscopy (NTEGRA Spectra Raman, λ = 473 nm). The BET principle was applied using a Sorbtometer M (Closed joint-stock company «Katakon», Russia) and ASAP 2400 V3.07 setups (Micromeritics Instrument Corporation, USA) devices for nitrogen adsorption/desorption measurements to establish the SSA.

2.4. Electrochemical Measurements

The active material (pure AGC or AGC modified with nickel hydroxide), carbon black (Timical Super C45), and poly (vinylidene fluoride) with N-methyl-two-pyrrolidone as a solvent in a mass ratio of 80:10:10 were mixed to prepare the electrodes. The homogenous slurry was applied to Ti foils in an area of 1 × 2 cm (2 cm^2). After then, electrodes were heated in a drying oven for 8 h at 120 °C. The procedure resulted in an average mass loading of 2.5 mg electrode material per square centimeter.

A two-electrode configuration with 6 molar potassium hydroxide as an electrolyte was used to evaluate the electrochemical characteristics of the electrodes. The obtained electrodes were used to run CV and GCD measurements using an electrochemical workstation (Elins P-45X). The CV and the GCD curves were used to calculate the specific capacitance of the capacitors [23].

3. Results

The yield of the carbonized carbon product, obtained from raw rice husk, after the pyrolysis carbonization step was 43.7 wt.%. After the thermochemical activation step, the yield of AGC reached 11 wt.%; the modest yield is in accordance with other authors [13,24] and is due to significant amounts of silica in rice husk [11]. As graphene shows excellent performance in supercapacitor applications and is furthermore promising for the introduction of the pseudo-capacitance material, it was intended to gain a significant amount of graphene in the activated carbon. Raman spectra of synthesized pure AGC are shown in Figure 1. As can be seen from the Raman spectra, there are three significant peaks: peak D at 1357 cm^{-1}, peak G at 1582 cm^{-1}, and peak 2D at 2717 cm^{-1}. These peaks are well known to be characteristic for graphene; furthermore, the intensity ratio between peak *G* (I_G) and peak *2D* (I_{2D}) allows to estimate the approximate number of graphene layers [25,26]. It can be stated with the Raman spectra in Figure 1 that few-layer graphene is present in the activated carbon samples.

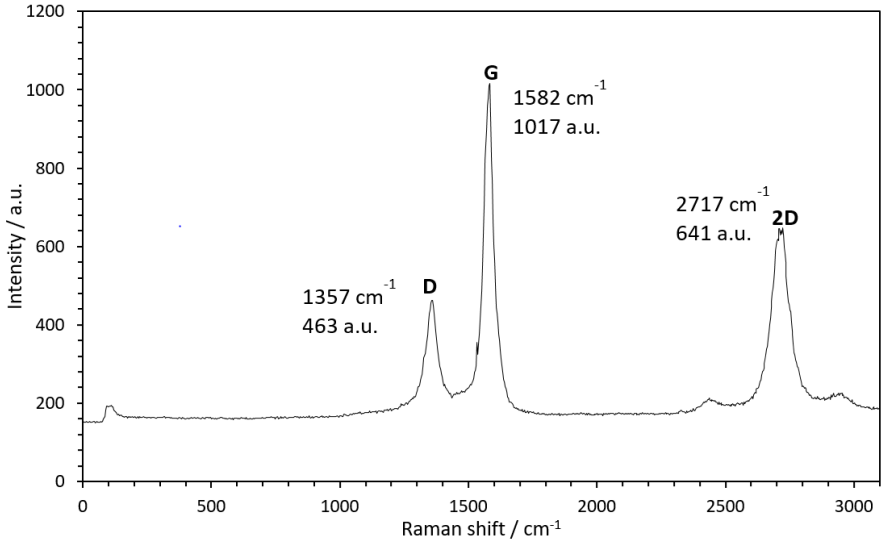

Figure 1. Raman spectra of activated rice husk (ARH), showing the three significant peaks (*D*, *G*, *2D*) for the presence and evaluation of graphene layers.

The structures of graphene layers derived from ARH were analyzed by transmission electron microscopy (TEM). A TEM image of graphene obtained from the rice husk of activation with KOH is shown in Figure 2. Micrographic images confirmed the synthesis of several layers of graphene. The produced samples consisted of clean-edge layers, containing defected and corrugated graphene structures. There are areas without defects, showing a homogeneous surface structure.

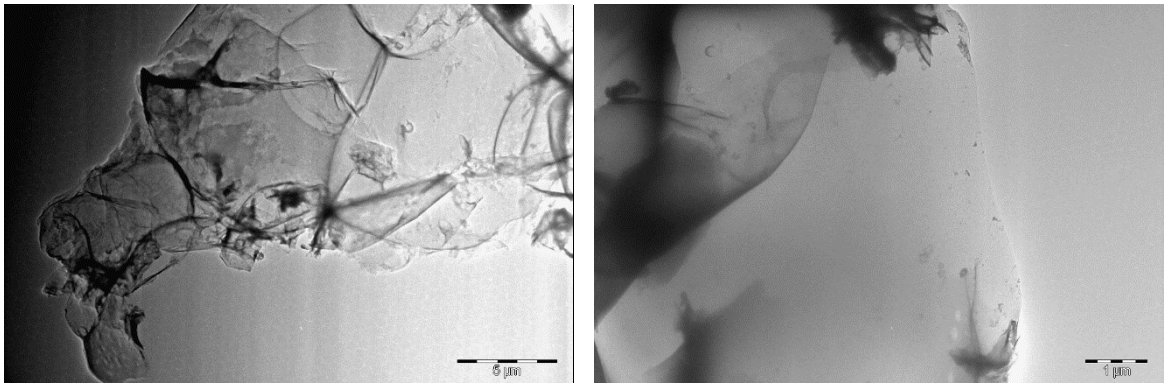

Figure 2. TEM images of ARH-derived graphene layers.

In Figure 3, SEM images of ARH are shown, the material exhibits a heterogenous structure changing between different shapes of porous surfaces. In Figure 3a, a porous sheet structure can be seen; the visible micro size pores show a wide variety. On the other hand, Figure 3b shows a surface with more homogenous round micropores with an average size of 15 μm. Small sites of pseudo-capacitive components on the surface and in the pores of the ARH could improve the specific capacitance of the material. Therefore, nickel hydroxide was chemically precipitated in a mixture of ARH. SEM micro-images of the resulting material are presented in Figure 3c,d. Particles with an average size of 2 μm, which fill up the bigger micropores, can be observed in Figure 3c,d. It can be presumed that these are nickel hydroxide particle aggregates that were built on the surface. Other authors also stated that nickel hydroxide precipitated on the AGC surface in the nanoscale range [27], which is probable but was not observable in this case.

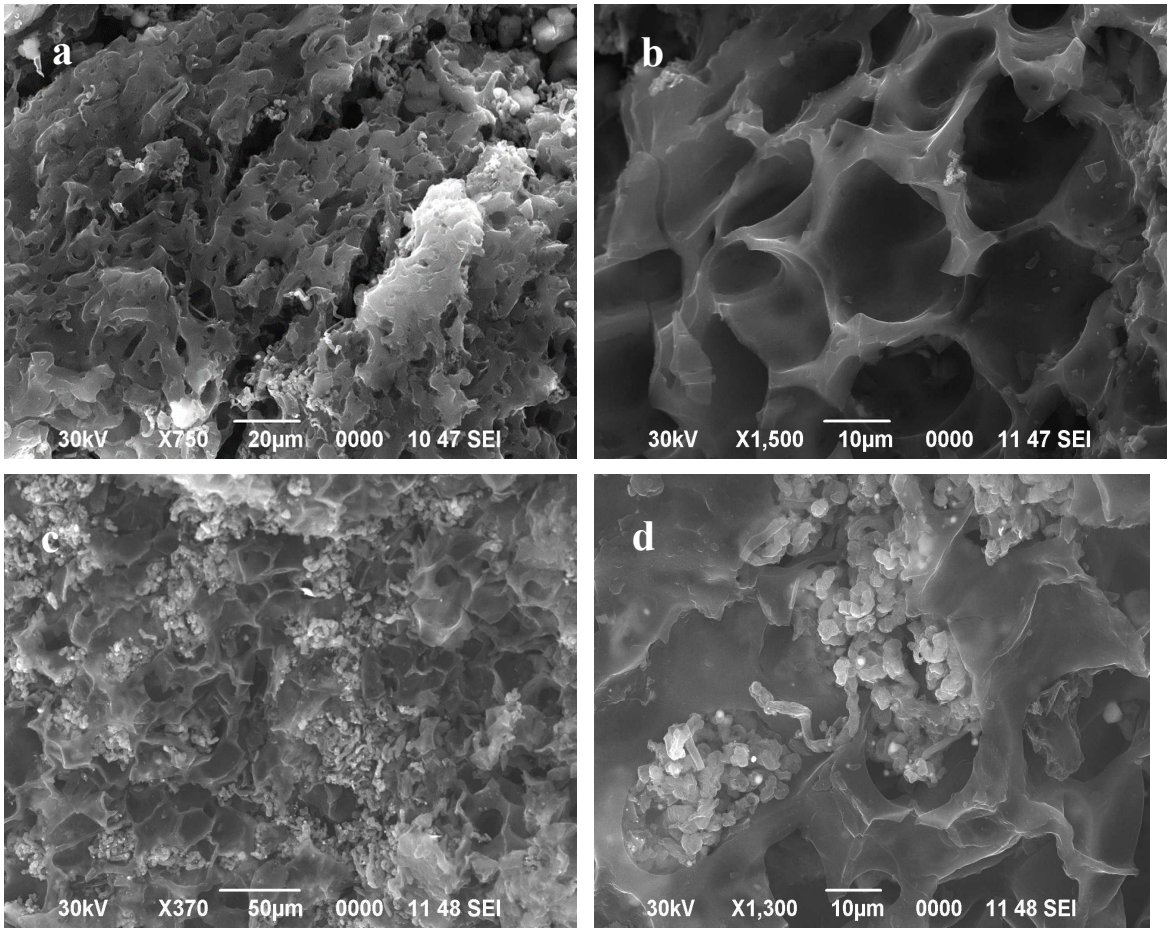

Figure 3. (**a**,**b**) SEM micro-images of ARH. (**c**,**d**) SEM micro-images of ARH after modification with 9 wt.% $Ni(OH)_2$.

The specific surface area is a crucial parameter in the preparation of high-performance supercapacitors. The SSA of AGC samples were investigated with N_2 adsorption/desorption measurements. Therein, a remarkable high SSA of around 3292 m^2 g^{-1} was found.

CV and GCD curves for the electrodes from the pure AGC and from AGC modified with 9 wt.% $Ni(OH)_2$ are presented in Figure 4. CV measurements have been conducted at various scanning rates in 6 M KOH for every prepared sample. The CV curves for both electrode pairs, pure AGC and $Ni(OH)_2$ modified show an almost rectangular shape, indicating that the composites are acting as excellent EDL capacitors. It is noteworthy that no Faradaic peak can be observed in the $Ni(OH)_2$ modified sample. Previously, some authors reported the dependence of capacitance values and the shape of the CV curves on the test cell configuration [28,29]. In the three-electrode cell configuration, capacitance values are twice higher than when using the two-electrode cell. The high sensitivity of three-electrode measurements can be misleading when projecting the energy storage capability of the real supercapacitor [30]. Therefore, a two-electrode configuration was used in this study. The cyclic voltammetry curves taken from the two-electrode cell configuration did not give defined Faradic peaks, which can be stated as the reason for the similarities in the CV shapes of the pure AGC and $Ni(OH)_2$ modified AGC. The CV curve of the sample modified with nickel hydroxide presents a larger rectangular area, indicating the higher specific capacitance of this sample (Figure 4b).

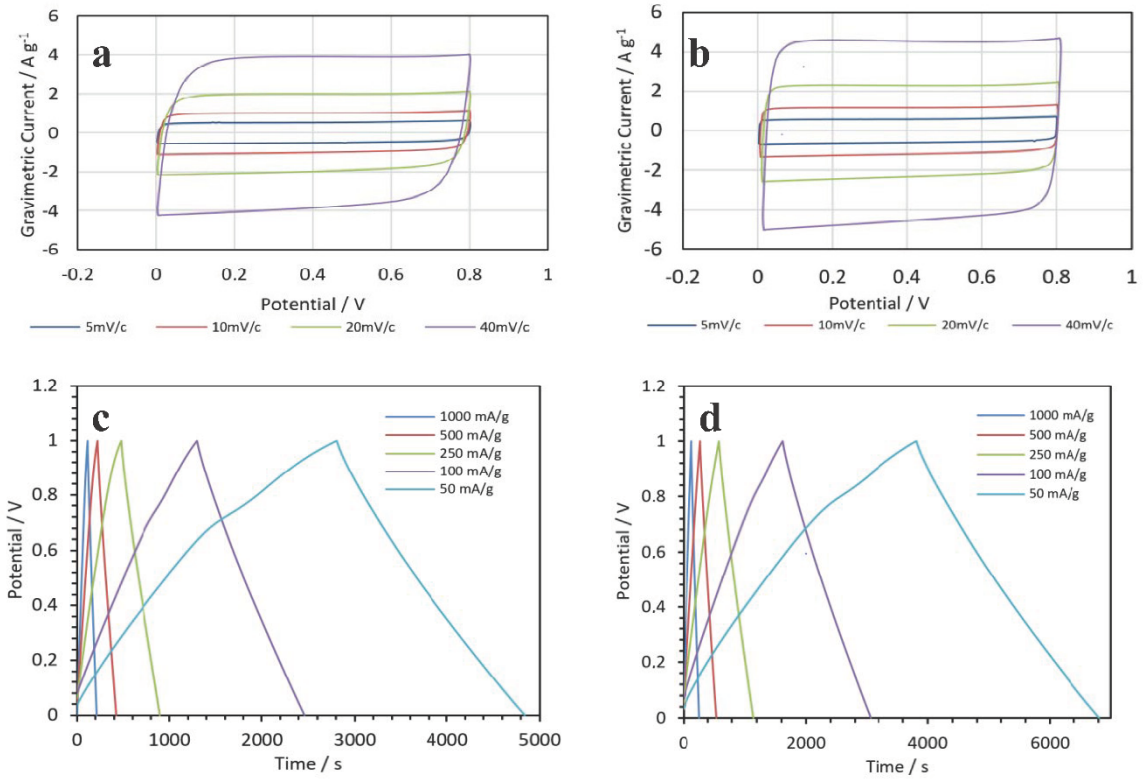

Figure 4. (**a**) CV of pure ARH electrodes. (**b**) CV of electrodes from ARH with 9 wt.% $Ni(OH)_2$. (**c**) GCD of electrodes from pure ARH. (**d**) GCD of electrodes from ARH with 9 wt.% $Ni(OH)_2$.

Different $Ni(OH)_2$ contents have been tested and the resulting capacitance, obtained from CV curves according to [23], are presented in Table 1. For pure AGC electrodes, a specific capacitance of 212 F g^{-1} at a scanning rate of 1 mV s^{-1} was found. The best results were reached with a theoretical weight content of 9% nickel hydroxide in the AGC, giving a specific capacitance of 258 F g^{-1} at a scanning rate of 1 mV s^{-1}. This is an increase of almost 22% compared to the pure AGC electrodes. When higher amounts of nickel hydroxide were added to the AGC, the specific capacitance started to drop again. This behavior was mainly due to the lowering of the EDLC capability by blocking the porosity of the pore opening of the AGC and the aggregation of $Ni(OH)_2$ [27]. The specific capacitance decreased with the increase in the scanning rate. This is the nature of electrochemical systems and can be ascribed to the diffusion limit of charge carriers. Figure 4 demonstrates the charge/discharge behavior of pure AGC and 9 wt.% $Ni(OH)_2$ on AGC electrodes in the potential range of 0–1000 mV in 6 M potassium hydroxide solution at different charge/discharge currents. The curves show a typical shape of isosceles triangles for EDLC, indicating high columbic efficiency. The curves for 9 wt.% nickel hydroxide (Figure 4d) and the pure AGC electrodes curve (Figure 4c) are similar in shape, which indicates the main contribution is made by the EDLC and not by pseudo-capacitance. It is clearly seen that the charge/discharge time for the 9 wt.% $Ni(OH)_2$ modified sample is longer than that of the pure AGC electrodes, thus illustrating that the specific capacitance is higher.

Table 1. Specific capacitance (F g^{-1}) of electrode material with different theoretical $Ni(OH)_2$ contents calculated from cyclic voltammetry (CV) curves. n.d.—not determined.

Scan Rate/mV s^{-1}	$Ni(OH)_2$ Content/wt.%				
	0	**4.5**	**9**	**13.5**	**18**
1	212	n.d.	258	n.d.	n.d.
5	202	213	236	182	172
10	187	206	230	177	163
20	178	200	225	173	153
40	176	194	218	168	142

The specific capacitance for pure AGC and 9 wt.% $Ni(OH)_2$ on AGC electrodes obtained from the GCD data according to [22] are presented in Table 2. The specific capacitance for the pure AGC electrodes at a current density of 50 mA g^{-1} was 236 F g^{-1}, whereas the 9 wt.% $Ni(OH)_2$ on the AGC electrodes showed a capacitance of 300 F g^{-1}. Consequently, the increase in the specific capacitance was 27%, an even higher value than the one calculated from the CV curves (22%).

Table 2. Specific capacitance (F g^{-1}) for pure ARH electrodes and electrodes from 9 wt.% $Ni(OH)_2$ on ARH calculated by using the GCD data.

Current Density/mA g^{-1}	Specific Capacitance/F g^{-1}	
	ARH	**9 wt.% $Ni(OH)_2$**
50	236	300
100	232	290
250	209	277
500	203	267
1000	197	256

In Table 2, it is clearly evident that the capacitance drops with the increase in current density. Other authors have ascribed this trend to the fact that some active surface sites become inapproachable for charge storage at higher current densities [2,30]. Usually, pseudo-capacitance materials show a higher loss of performance with increasing current densities [2]. However, the electrodes from the pure AGC and the 9 wt.% $Ni(OH)_2$ on AGC showed similar behavior in decreasing the capacitance with increasing current densities. Moreover, the decrease of the specific capacitance was 12–15% for the increase of current density by a factor of 10 (100→1000 mA g^{-1}), which indicates good high-rate performance.

The GCD test was carried out at the current density of 2000 mA g^{-1} after 2000 cycles to truly reflect the electrochemical characteristics of the supercapacitor with the AGC electrodes modified with 9 wt.% $Ni(OH)_2$ (Figure 5a). At this current density, the specific capacitance for the modified electrodes was calculated to be 236 F g^{-1}. Figure 5a also shows the voltage drop of the device at the discharge start. The internal resistance R_{inter} calculated from the drop voltage ΔV at the time of discharge start was 0.78 Ohm.

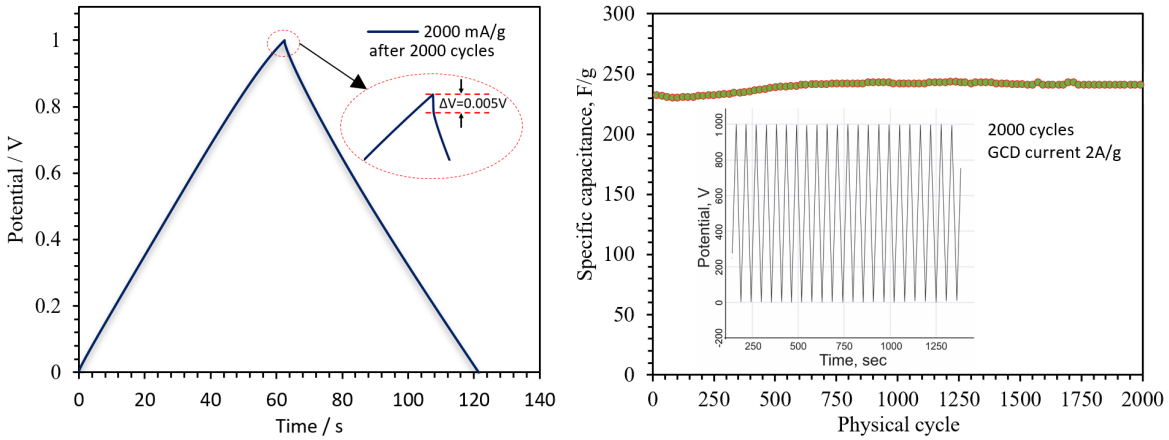

(**a**) (**b**)

Figure 5. (**a**) GCD curve at 2000 mA g^{-1} after 2000 cycles for the device with AGC with 9 wt.% $Ni(OH)_2$ electrodes (**b**) Capacity retention test of the device with AGC with 9 wt.% $Ni(OH)_2$ electrodes.

A cyclic charging and discharging test was performed for a few thousands of cycles to determine the physicochemical stability of the electrodes in the 6 M KOH electrolyte. Figure 5b shows the capacitance retention of the supercapacitor with AGC electrodes modified with 9 wt.% $Ni(OH)_2$. From the graph, it can be seen that the capacitance of the device slightly increased from the 1st to the 600th cycle. The device demonstrated very stable performance throughout the testing process after the 600th cycle.

4. Conclusions

In summary, porous carbon or so-called activated carbon was successfully synthesized by using rice husk as a renewable biomass waste. The obtained material showed a very high SSA of 3292 m^2 g^{-1} by BET analysis. Raman spectra and TEM of the AGC indicated that the composite contained few-layer graphene. The specific capacitance of pure AGC electrodes, obtained from CV data, was 212 F g^{-1} at a scanning rate of 1 mV s^{-1}. The GCD data showed a specific capacitance of 236 F g^{-1} at a current density of 50 mA g^{-1}. With a simple chemical precipitation method, different quantities of $Ni(OH)_2$ were deposited on the AGC surface. The surface of the pure AGC, as well as the $Ni(OH)_2$ modified samples, were studied with SEM and nitrogen adsorption/desorption measurements, showing a highly porous surface area. It was found that theoretical amounts of about 9 wt.% $Ni(OH)_2$ on AGC exhibited the best results when it came to the specific capacitance. The specific capacitance of 9 wt.% $Ni(OH)_2$ on AGC electrodes, calculated from the CV data, was 258 F g^{-1} at a scanning rate of 1 mV s^{-1}. The GCD data showed a specific capacitance of 300 F g^{-1} at a current density of 50 mA g^{-1}, which is an increase of 22% in the case of the CV data and 27 % when calculated with the GCD data. The AGC electrodes modified with 9 wt.% $Ni(OH)_2$ were tested up to 2000 charge–discharge cycles without changing the operational characteristics. In addition, the AGC electrodes modified with 9 wt.% $Ni(OH)_2$ showed very good structural integrity and stability during the testing with up to 2000 charge–discharge cycles.

Author Contributions: Conceptualization: M.Y. and C.S.; validation and formal analysis: T.T.; investigation: C.D. and A.T.; writing—original draft preparation: F.S. and M.Y.; writing—review and editing: N.P. and S.K.; project administration: B.L. All authors have read and agreed to the published version of the manuscript.

Funding: This research was supported by the Ministry of Education and Science of the Republic of Kazakhstan in the framework of the scientific and technology Program AP05133792-OT-18.

Acknowledgments: Makpal Seitzhanova, Gauhar Smagulova, and Bagdat Rakhymetov for their technical assistance in the laboratory.

Conflicts of Interest: The authors declare no conflict of interest.

References

1. Luo, X.; Wang, J.; Dooner, M.; Clarke, J. Overview of current development in electrical energy storage technologies and the application potential in power system operation. *Appl. Energy* **2015**, *137*, 511–536. [CrossRef]
2. Quan, H.; Cheng, B.; Xiao, Y.; Lei, S. One-pot synthesis of α-Fe_2O_3 nanoplates-reduced graphene oxide composites for supercapacitor application. *Chem. Eng. J.* **2016**, *286*, 165–173. [CrossRef]
3. Zou, Z.; Cao, J.; Cao, B.; Chen, W. Evaluation strategy of regenerative braking energy for supercapacitor vehicle. *ISA Trans.* **2015**, *55*, 234–240. [CrossRef] [PubMed]
4. Zhang, X.; Shi, W.; Zhu, J.; Zhao, W.; Ma, J.; Mhaisalkar, S.; Maria, T.L.; Yang, Y.; Zhang, H.; Hng, H.H.; et al. Synthesis of porous NiO nanocrystals with controllable surface area and their application as supercapacitor electrodes. *Nano Res.* **2010**, *3*, 643–652. [CrossRef]
5. Ansari, S.A.; Fouad, H.; Ansari, S.G.; Sk, M.P.; Cho, M.H. Mechanically exfoliated MoS_2 sheet coupled with conductive polyaniline as a superior supercapacitor electrode material. *J. Colloid Interface Sci.* **2017**, *504*, 276–282. [CrossRef]
6. Pavlenko, V.V.; Abbas, Q.; Przygocki, P.; Lesbayev, B.T.; Mansurov, Z.A. Temperature dependent characteristics of activated carbons from walnut shells for improved supercapacitor performance. *Eurasian Chem. Technol. J.* **2018**, *20*, 99–105. [CrossRef]
7. Sultanov, F.; Bakbolat, B.; Mansurov, Z.; Pei, S.-S.; Ebrahim, R.; Daulbayev, C.; Urazgaliyeva, A.; Tulepov, M. Spongy Structures Coated with Carbon Nanomaterialsfor Efficient Oil/Water Separation. Eurasian Chem. *Technol. J.* **2017**, *19*, 127.
8. Sultanov, F.; Bakbolat, B.; Daulbaev, C.; Urazgalieva, A.; Azizov, Z.; Mansurov, Z.; Tulepov, M.; Pei, S.S. Sorptive Activity and Hydrophobic Behavior of Aerogels Based on Reduced Graphene Oxide and Carbon nanotubes. *J. Eng. Phys. Thermophys.* **2017**, *90*, 826–830. [CrossRef]
9. Zhi, M.; Xiang, C.; Li, J.; Li, M.; Wu, N. Nanostructured carbon–metal oxide composite electrodes for supercapacitors: A review. *Nanoscale* **2013**, *5*, 72–88. [CrossRef]
10. Temirgaliyeva, T.S.; Kuzuhara, S.; Noda, S.; Nazhipkyzy, M.; Kerimkulova, A.R.; Lesbayev, B.T.; Prikhodko, N.G.; Mansurov, Z.A. Self-Supporting Hybrid Supercapacitor Electrodes Based on Carbon Nanotube and Activated Carbons. *Eurasian Chem. Technol. J.* **2018**, *20*, 169–175. [CrossRef]
11. Yuan, C.; Lin, H.; Lu, H.; Xing, E.; Zhang, Y.; Xie, B. Synthesis of hierarchically porous MnO_2/rice husks derived carbon composite as high-performance electrode material for supercapacitors. *Appl. Energy* **2016**, *178*, 260–268. [CrossRef]
12. He, X.; Ling, P.; Yu, M.; Wang, X.; Zhang, X.; Zheng, M. Rice husk-derived porous carbons with high capacitance by $ZnCl_2$ activation for supercapacitors. *Electrochim. Acta* **2013**, *105*, 635–641. [CrossRef]
13. Seitzhanova, M.A.; Chenchik, D.I.; Yeleuov, M.A.; Mansurov, Z.A.; Di Capua, R.; Elibaeva, N.S. Synthesis and characterization of graphene layers from rice husks. *Chem. Bull. Kazakh Natl. Univ.* **2018**, 12–18. [CrossRef]
14. Seitzhanova, M.A.; Mansurov, Z.A.; Yeleuov, M.; Roviello, V.; Di Capua, R. The Characteristics of Graphene Obtained from Rice Husk and Graphite. *Eurasian Chem. Technol. J.* **2019**, *21*, 149–156. [CrossRef]
15. Muramatsu, H.; Kim, Y.A.; Yang, K.S.; Cruz-Silva, R.; Toda, I.; Yamada, T.; Terrones, M.; Endo, M.; Hayashi, T.; Saitoh, H. Rice husk-derived graphene with nano-sized domains and clean edges. *Small* **2014**, *10*, 2766–2770. [CrossRef]
16. He, Y.; Chen, W.; Li, X.; Zhang, Z.; Fu, J.; Zhao, C.; Xie, E. Freestanding three-dimensional graphene/MnO_2 composite networks as ultralight and flexible supercapacitor electrodes. *ACS Nano* **2013**, *7*, 174–182. [CrossRef] [PubMed]
17. Dong, X.C.; Xu, H.; Wang, X.W.; Huang, Y.X.; Chan-Park, M.B.; Zhang, H.; Wang, L.H.; Huang, W.; Chen, P. 3D graphene–cobalt oxide electrode for high-performance supercapacitor and enzymeless glucose detection. *ACS Nano* **2012**, *6*, 320–3213. [CrossRef]
18. Gong, M.; Zhou, W.; Tsai, M.C.; Zhou, J.; Guan, M.; Lin, M.C.; Pennycook, S.J. Nanoscale nickel oxide/nickel heterostructures for active hydrogen evolution electrocatalysis. *Nat. Commun.* **2014**, *5*, 1–6. [CrossRef]
19. Liu, J.; Chen, M.; Zhang, L.; Jiang, J.; Yan, J.; Huang, Y.; Lin, J.; Fan, H.J.; Shen, Z.X. A flexible alkaline rechargeable Ni/Fe battery based on graphene foam/carbon nanotubes hybrid film. *Nano Lett.* **2014**, *14*, 7180–7187. [CrossRef]

20. Tang, Z.; Tang, C.H.; Gong, H. A high energy density asymmetric supercapacitor from nano-architectured $Ni(OH)_2$/carbon nanotube electrodes. *Adv. Funct. Mater.* **2012**, *22*, 1272–1278. [CrossRef]
21. Yang, G.W.; Xu, C.L.; Li, H.L. Electrodeposited nickel hydroxide on nickel foam with ultrahigh capacitance. *Chem. Commun.* **2008**, *48*, 6537–6539. [CrossRef] [PubMed]
22. Hu, G.; Li, C.; Gong, H. Capacitance decay of nanoporous nickel hydroxide. *J. Power Sources* **2010**, *195*, 6977–6981. [CrossRef]
23. Wang, C.; Xu, J.; Yuen, M.F.; Zhang, J. Hierarchical Composite Electrodes of Nickel Oxide Nanoflake 3D Graphene for Hig-Performance Pseudocapacitors. *Adv. Funct. Mater.* **2014**, *24*, 6372–6380. [CrossRef]
24. Cheah, W.K.; Ooi, C.H.; Yeoh, F.Y. Rice husk and rice husk ash reutilization into nanoporous materials for adsorptive biomedical applications: A review. *Open Mater. Sci.* **2016**, *3*, 27–38. [CrossRef]
25. Prikhod'ko, N.A.; Mansurov, Z.A.; Auelkhankyzy, M.; Lesbaev, B.T.; Nazhipkyzy, M.; Smagulova, G.T. Flame Synthesis of Graphene Layers at Low Presssure. *Russ. J. Phys. Chem. B* **2015**, *9*, 743–747. [CrossRef]
26. Ferrari, A.C. Raman spectroscopy of graphene and graphite: Disorder, electron–phonon coupling, doping and nonadiabatic effects. *Solid State Commun.* **2017**, *143*, 47–57. [CrossRef]
27. Huang, Q.; Wang, X.; Li, J.; Dai, C.; Gamboa, S.; Sebastian, P.J. Nickel hydroxide/activated carbon composite electrodes for electrochemical capacitors. *J. Power Sources* **2007**, *164*, 425–429. [CrossRef]
28. Stoller, M.D.; Ruoff, R.S. Best practice methods for determining an electrode material's performance for ultracapacitors. *Energy Environ. Sci.* **2010**, *3*, 1294–1301. [CrossRef]
29. Khomenko, V.; Frackowiak, E.; Beguin, F. Determination of the specific capacitance of conducting polymer/nanotubes composite electrodes using different cell configurations. *Electrochim. Acta* **2005**, *50*, 2499–2506. [CrossRef]
30. Dubal, D.P.; Kim, J.G.; Kim, Y.; Holze, R.; Lokhande Ch, D.; Kim, W.B. Supercapacitors Based on Flexible Substrates: An Overview. *Energy Technol.* **2014**, *2*, 325–341. [CrossRef]